Subunit-specific Contribution of Pore-forming Domains to NMDA Receptor Channel Structure and Gating

Alexander I. Sobolevsky, Michael L. Prodromou, Maria V. Yelshansky, and Lonnie P. Wollmuth

Department of Neurobiology and Behavior, State University of New York at Stony Brook, Stony Brook, NY 11794

N-methyl-D-aspartate receptors (NMDARs) are ligand-gated ion channels that contribute to fundamental physiological processes such as learning and memory and, when dysfunctional, to pathophysiological conditions such as neurodegenerative diseases, stroke, and mental illness. NMDARs are obligate heteromultimers typically composed of NR1 and NR2 subunits with the different subunits underlying the functional versatility of NMDARs. To study the contribution of the different subunits to NMDAR channel structure and gating, we compared the effects of cysteine-reactive agents on cysteines substituted in and around the M1, M3, and M4 segments of the NR1 and NR2C subunits. Based on the voltage dependence of cysteine modification, we find that, both in NR1 and NR2C, M3 appears to be the only transmembrane segment that contributes to the deep (or voltage dependent) portion of the ion channel pore. This contribution, however, is subunit specific with more positions in NR1 than in NR2C facing the central pore. Complimentarily, NR2C makes a greater contribution than NR1 to the shallow (or voltage independent) portion of the pore with more NR2C positions in pre-M1 and M3-S2 linker lining the ion-conducting pathway. Substituted cysteines in the M3 segments in NR1 and NR2C showed strong, albeit different, state-dependent reactivity, suggesting that they play central but structurally distinct roles in gating. A weaker state dependence was observed for the pre-M1 regions in both subunits. Compared to M1 and M3, the M4 segments in both NR1 and NR2C subunits had limited accessibility and the weakest state dependence, suggesting that they are peripheral to the central pore. Finally, we propose that Lurcher mutation-like effects, which were identified in and around all three transmembrane segments, occur for positions located at dynamic protein–protein or protein–lipid interfaces that have state-dependent accessibility to methanethiosulfonate (MTS) reagents and therefore can affect the equilibrium between open and closed states following reactions with MTS reagents.

The Journal of General Physiology

INTRODUCTION

The *N*-methyl-D-aspartate (NMDA) receptor subtype of ionotropic glutamate receptors (GluRs) mediates a slow synaptic response at the majority of excitatory synapses in the brain. Diverse gating properties as well as regulation by a variety of extracellular (e.g., Zn^{2+}, Mg^{2+}, pH, redox agents) and intracellular (e.g., Ca^{2+}, Ca^{2+}/calmodulin, tyrosine kinases) signals, proteins (e.g., PSD-95), and physical stimuli (membrane tension, light) underlie a unique contribution of NMDARs to key physiological processes such as learning and memory and to pathological conditions such as neurodegenerative diseases, stroke, and mental illness (Dingledine et al., 1999). Given this diverse functional regulation, the structure of the NMDAR channel presumably is also complex.

Functional NMDARs are obligate heteromultimers typically formed by NR1 and NR2 subunits (see, however, Chatterton et al., 2002). While there is a single NR1 subunit, there are four subtypes of NR2 subunits (NR2A, NR2B, NR2C, and NR2D) with the resulting NR1-NR2 heteromers having different functional properties such as kinetics, single channel conductance and ion channel block (Monyer et al., 1994; Kuner and Schoepfer, 1996; Vicini et al., 1998; Wyllie et al., 1998; Banke and Traynelis, 2003; Cull-Candy and Leszkiewicz, 2004; Auerbach and Zhou, 2005; Clarke and Johnson, 2006). Similar to AMPA receptors, NMDAR subunits form tetramers assembled together as dimer-of-dimers (Mayer, 2006) with the major building block being an NR1-NR2 dimer (Furukawa et al., 2005). The relative arrangement of subunits in two dimers is unknown though it has been proposed (Schorge and Colquhoun, 2003; Furukawa et al., 2005) that like subunits are adjacent to each other in the mature receptor (1-1-2-2 arrangement).

Both NR1 and NR2 contribute to the formation of the NMDAR ion channel (Fig. 1 A). This contribution, however, is not identical. In NMDARs, the inner or cytoplasmic vestibule of the channel is formed mainly by the cytoplasmic reentrant M2 loops with the channel's narrow constriction formed by nonhomologous asparagines located at or near the tip of the loop (Kuner et al., 1996;

Correspondence to Lonnie P. Wollmuth: lwollmuth@notes1.cc.sunysb.edu

A.I. Sobolevsky's present address is Vollum Institute, Oregon Health and Science University, L474, 3181 SW Sam Jackson Park Road, Portland, OR 97239-3098.

Abbreviations used in this paper: APV, DL-2-amino-5-phosphonopentanoic acid; GluR, glutamate receptor; MTS, methanethiosulfonate; MTSEA, 2-aminoethyl methanethiosulfonate; MTSET, 2-(trimethylammonium)ethyl methanethiosulfonate; NMDAR, *N*-methyl-D-aspartate receptor; PTrEA, 3-(triethylammonium) propyl methanethiosulfonate; SCAM, substituted cysteine accessibility method.

Wollmuth et al., 1996). The outer cavity (also referred to as the extracellular vestible), as contributed by the NR1 subunit, is formed by regions in and around the transmembrane segments M1, M3, and M4, with M3 forming the core of this cavity leading up to the channel's narrow constriction and regions N terminal to M1 (pre-M1) and M4 (pre-M4) and regions C terminal to M3 forming more superficial parts (Beck et al., 1999; Sobolevsky et al., 2002a). The M3 segment of NR2 also contributes to the core of the outer cavity but NR2 positions are apparently located approximately four amino acid residues (a turn of an α-helix) more external than homologous ones in NR1 (Sobolevsky et al., 2002b). This staggering of the M3 segments may underlie the differential contribution of the NR1 and NR2 subunits to Ca^{2+} permeability (Watanabe et al., 2002) and channel block (Kashiwagi et al., 2002; Jin et al., 2007). Nevertheless, despite the importance of M3 to channel gating (e.g., Kohda et al., 2000; Jones et al., 2002; Sobolevsky et al., 2002a; Low et al., 2003; Yuan et al., 2005), the relative contribution and orientation of the NR1 and NR2 M3 segments remains unknown. Also unknown is the contribution of the NR2 M1 and M4 segments to pore structure and channel gating. This information is essential for unraveling the structural basis of NMDAR channel permeation and block, and the functional asymmetry between NR1 and NR2 subunits during activation (Banke and Traynelis, 2003).

To study the contribution of different domains to NMDAR channel structure and gating, we measured the accessibility and reaction rates of cysteines substituted in and around the M1, M3, and M4 segments of the NR2C subunit with cysteine-reactive agents and compared them to those in NR1 (Beck et al., 1999; Sobolevsky et al., 2002a). Gating in GluRs, as considered in the present manuscript, refers to the process whereby conformational changes in the ligand-binding domain induced by the coagonists glutamate and glycine are converted to channel opening/closure. In terms of gating, GluRs, including NMDARs, exist in three major conformational states: open, closed, and desensitized. To simplify our studies, we chose the NR2C subtype of the NR2 subunit because NMDARs composed of the NR1-NR2C subunits show no apparent desensitization (Krupp et al., 1996), making it easier to study activation gating of NMDAR channel separately from desensitization gating. Our results suggest that the pre-M1 and M3 segments make a central, though asymmetric and subunit-specific, contribution to the structure of the central pore in NMDARs. The M4 segments are most likely located more peripheral to the central pore but play a unique and indispensable structural role.

MATERIALS AND METHODS

Mutagenesis and Expression

Mutations made in and around the M1, M3, and M4 segments of the NR1 subunit (Beck et al., 1999) as well as in the M3 segment (W613C-I633C) of the NR2C subunit (Sobolevsky et al., 2002b) were described previously. Cysteine substitutions in and around the M1 and M4 segments and the M3-S2 linker of the NR2C subunit (see legend to Fig. 1) were generated either with QuickChange site-directed mutagenesis kit (Stratagene) or by other PCR-based methods using Platinum Pfx DNA polymerase (Invitrogen) or Pfu poly DNA polymerase (Stratagene). Subsequently, a fragment encompassing the mutation was subcloned back into the wild-type template. All constructs were sequenced over the entire length of the replaced fragment. cRNA was transcribed for each expression construct using SP6 RNA polymerase (Ambion Inc.) and examined electrophoretically on a denaturating agarose gel. Dilutions of RNA (0.01–0.1 μg/μl) were prepared in order to achieve optimal expression. Wild-type and mutant NR1 and NR2C subunits were coexpressed in *Xenopus laevis* oocytes. Oocytes were prepared, injected, and maintained as previously described (Wollmuth et al., 1996; Sobolevsky et al., 2002a). Recordings were made 2–5 d after injections.

Current Recordings and Data Analysis

Whole-cell currents of *Xenopus* oocytes were recorded at room temperature (20–23°C) using two-electrode voltage clamp (DAGAN TEV-200A, DAGAN Corp.) with Cell Works software (*npi* electronic). Microelectrodes were filled with 3 M KCl and had resistances of 1–4 MΩ. To minimize solution exchange rates, we used a narrow flowthrough recording chamber with a small volume of ~70 μl. The external solution consisted of (in mM) 115 NaCl, 2.5 KCl, 0.18 $CaCl_2$, and 5 HEPES (pH 7.2, NaOH). All reagents, including glutamate (200 μM), glycine (20 μM), DL-2-amino-5-phosphonopentanoic acid (APV) (100 μM), and cysteine-reactive agents (see below), were applied with the bath solution. All chemicals, unless otherwise noted, were obtained from Sigma-Aldrich.

Data analysis was done using Igor Pro (WaveMetrics, Inc.), Microcal Origin 4.1, and Microsoft Excel. For analysis and illustration of kinetic experiments, leak currents were subtracted from total currents. Results are presented as mean ± SEM. An ANOVA or Student's *t* test was used to define statistical differences. The Tukey test was used for multiple comparisons. Significance was assumed if $P < 0.05$.

Experimental Protocols

NMDAR cysteine-substituted mutant channels were probed from the extracellular side of the membrane with various cysteine-reactive agents, including the positively charged methanethiosulfonate (MTS) reagents 2-aminoethyl MTS (MTSEA), 2-(trimethylammonium)ethyl MTS (MTSET), and 3-(triethylammonium) propyl MTS (PTrEA). MTS-containing solutions were prepared, stored, and applied as previously described (Sobolevsky et al., 2002a). MTS reagents were purchased from Toronto Research Chemicals, Inc.

Steady-State Reactions. Steady-state reactions were quantified at –60 mV (see Fig. 2, A–C). Baseline agonist-activated current amplitudes (I_{pre}) were established by three to five consecutive 15-s applications of glutamate and glycine separated by 60 to 120-s washes in glutamate-free solution. Subsequent to the last wash, an MTS reagent (2 mM) was applied for 60 s either in presence of agonists or in their absence (but in the presence of APV). After the cysteine-reactive agent exposure, current amplitudes (I_{post}) were determined again using three to five agonist applications. The washout interval between the end of the cysteine-reactive agent application and the first post agonist application ranged from 1.25 to 5 min. The change in the agonist-activated current amplitude, expressed as a percentage (% change), was calculated as: $=(1 - I_{post}/I_{pre}) \times 100$. The steady-state change in the leak current amplitude, expressed as a percentage (Δ leak), was calculated

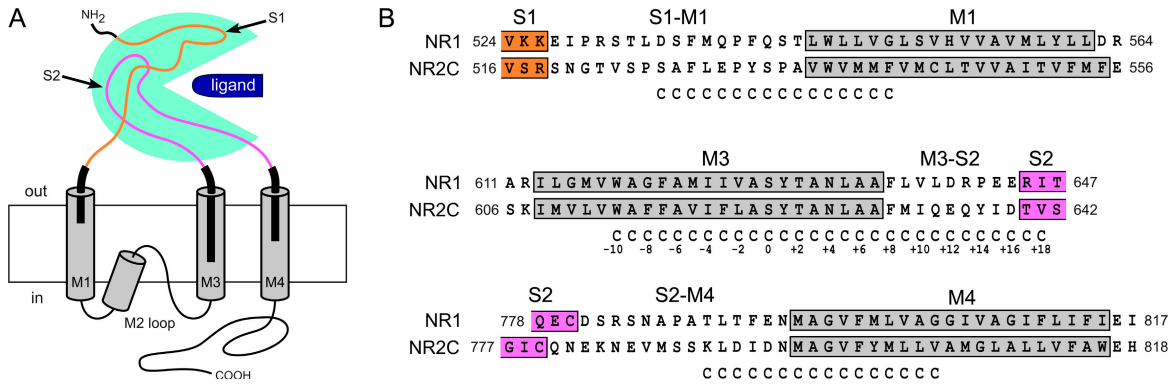

Figure 1. Membrane topology of NMDAR NR1 and NR2C subunits. (A) Topology of a NMDAR subunit. Hydrophobic and presumed α-helical membrane spanning segments M1, M3, and M4 and the C-terminal half of the M2 pore loop are shown as gray cylinders. The S1 (N terminal to M1) (highlighted in orange) and S2 (between M3 and M4) (highlighted in magenta) lobes comprise the ligand-binding core, a crystal structure of which exists for NR1-NR2A (Furukawa et al., 2005). The thick black bars indicate regions where cysteines were substituted. In all plots subsequent to Fig. 1, presumed transmembrane segments are highlighted in gray with their extracellular side pointing upward. (B) Sequence alignment of regions encompassing the transmembrane domains in NMDAR NR1 and NR2C subunits. The transmembrane segments M1, M3, and M4 are highlighted in gray, whereas proximal parts of S1 and S2 are highlighted in orange and magenta, respectively. Previously described (M3: W613C-I633C) (Sobolevsky et al., 2002b) and newly made (M1, S526C-F541C; M3-S2 linker, Q634C-V641C; and M4, K790C-V805C) single cysteine substitutions in the NR2C subunit are indicated (CC…CC). Numbering is for the mature protein. For M3, we also used a relative numbering system where the serine (S) in the highly conserved SYTANLAAF motif is designated "0" with positions more N or C terminal indicated by negative or positive numbers, respectively.

as: $=((I_{leak\_pre} - I_{leak\_post})/(I_{pre} + I_{leak\_pre})) \times 100$, where I_{leak_pre} and I_{leak_post} are the leak current amplitudes before and after the MTS reagent application, respectively. Although this equation is not necessarily intuitive, we used it in this form since inhibition and potentiation of glutamate-activated currents (% change) and decreases and increases in leak current (Δ leak) are given the same positive and negative signs, respectively.

Reaction Rates. Reaction rates in the presence of glutamate and glycine (k) and in their absence but in the presence of APV (k_{APV}) were determined using "pulsive" protocols (see Fig. 3 A and Fig. 9 A) as described in detail in Sobolevsky et al. (2002b). In brief, changes in current amplitudes were fitted with a single exponential. The reciprocal of the time constant of this fit multiplied by the concentration of the MTS reagent defined the apparent second-order rate constant for chemical modification. Since the highest MTS concentrations we were able to use without causing nonspecific effects on oocytes membranes were in the low millimolar range ($\sim 10^{-3}$ M) and a reasonable experimental time without significant rundown of current amplitudes was on the order of tens of minutes ($\sim 10^3$ s), we considered 1 $M^{-1}s^{-1}$ to be the limit of resolution for our kinetic experiments. The voltage dependence of k was analyzed according to the following equation:

$$k = k_0 \exp(-z\delta F V_h / RT), \quad (1)$$

where V_h is the holding potential, k_0 is the apparent second order rate constant for modification at $V_h = 0$, δ is the fraction of the transmembrane electric field the MTS reagent passes to reach the exposed cysteine, and z is the charge of the reagent. F, R, and T have their usual meaning. To derive $z\delta$, we rearranged Eq. 1:

$$-(RT/F)\ln k = A + z\delta V_h, \quad (2)$$

where A is $-(RT/F)\ln k_0$, and fitted Eq. 2 to plots of $-(RT/F)\ln k$ against V_h with free parameters A and $z\delta$.

Quantification of Coverage in Helical Nets. A helical net is built based on the assumption of 3.6 amino acid residues per turn of an α-helix with a constant angular difference of 100° between two consecutive positions. To quantify MTS reagent-accessible surfaces of α helices, we first defined a neighboring position as one of the six positions surrounding a selected one on the surface of an α-helix: two positions, the preceding and following ones in the polypeptide chain that belong to the same turn of the α-helix, and the two closest positions in the turn below (two positions) and in the turn above (two positions). Then, we grouped neighboring positions with common functional properties (e.g., effect of MTS reagents on glutamate-activated current amplitudes or voltage dependence of modification rates) into clusters. We defined the angular width of a cluster as the size of the smallest sector that is covered by this cluster on the surface of the corresponding α-helix and calculated it as a difference between two extreme angular values for positions within the cluster. For example, the angular width of the dark blue cluster in NR1 M3 (Fig. 4 A) is 260° (=280°(A + 3) − 20°(N+4)), while the same value for the dark blue cluster in NR2C M3 is 60° (=140°(V − 5) − 80°(L − 2)).

RESULTS

To study the contribution of the NR1 and NR2C subunits to NMDAR channel structure and gating, we recorded currents activated by coapplication of glutamate (200 μM) and glycine (20 μM) (referred to as glutamate-activated currents) from oocytes expressing combinations of wild-type and cysteine-substituted NR1 and NR2C subunits. Since NMDARs composed of the NR1-NR2C subunits show no apparent desensitization (Krupp et al., 1996), we assume that these cysteine-substituted NR1-NR2C receptors exist primarily in the closed (absence of glutamate and glycine) or in the closed and open (presence of glutamate and glycine) states. Cysteine substitutions in the M1 and M4 segments of

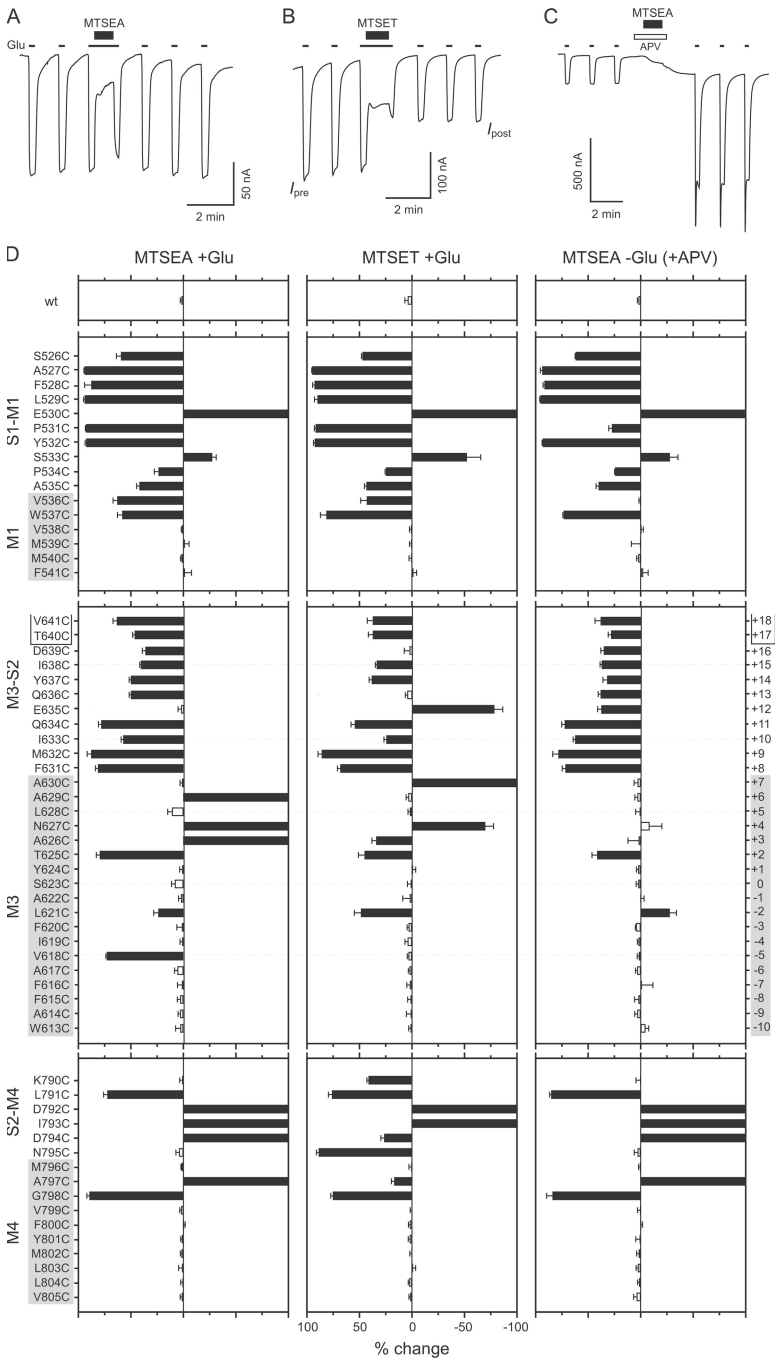

Figure 2. Accessibility of substituted cysteines in NR2C to MTS reagents. (A–C) Protocols to assay accessibility of substituted cysteines in the presence (A and B) or absence (C) of glutamate and glycine using steady-state reactions (see Materials and Methods). (A and B) The examples show whole-cell currents recorded from *Xenopus* oocytes expressing wild-type (wt) NR1-NR2C (A) or NR1-NR2C(A535C) (B) channels. Currents were elicited by glutamate (200 μM) and glycine (20 μM) (thin lines) at a holding potential (V_h) of −60 mV. MTSEA (A) or MTSET (B) (2 mM, thick lines) was applied for 60 s in the continuous presence of coagonists. (C) NR1-NR2C(A797C) channels were probed with MTSEA (2 mM, thick line) applied for 60 s in the continuous presence of the competitive NMDAR antagonist APV (100 μM, open box). (D) Mean percent change (% change) in glutamate-activated current amplitudes measured before (I_{pre}) and after (I_{post}) exposure to MTSEA (MTSEA + Glu) or MTSET (MTSET + Glu) in the presence of glutamate/glycine, or MTSEA in the absence of coagonists but in the continuous presence of APV (MTSEA – Glu). Left and right pointing bars indicate inhibition and potentiation, respectively ($n > 4$). For positions with % change = −100, potentiation was stronger than 100%. The MTSEA + Glu data for positions W613C-I633C (W-10 to I+10) in the NR2C M3 are from Sobolevsky et al. (2002b). Filled bars indicate that the value of % change is statistically different from zero. Open-ended box encompassing T640C and V641C indicates that these positions belong to S2.

the NR1 subunit as well as in the M3 segments of the NR1 and NR2C subunits were described previously (Beck et al., 1999; Sobolevsky et al., 2002a) (see Materials and Methods). In the present study, we generated 40 new mutant NR2C subunits that have single cysteine substitutions in regions encompassing the N-terminal end of M1 including the proximal part of the S1-M1 linker (also referred to as pre-M1), the M3-S2 linker, and the N-terminal end of the M4 segment including the proximal part of the S2-M4 linker (also referred to as pre-M4) (Fig. 1 B).

Steady-State Reactions of Substituted Cysteines in NR2C with MTS Reagents

Figs. 2 (A–C) illustrates our protocols to determine steady-state reactivity of substituted cysteines with MTS reagents. To measure reactivity, we compared the amplitude of the current activated by the coapplication of glutamate and glycine (thin lines) before (I_{pre}) and after (I_{post}) exposure to MTS reagents (2 mM, thick lines). The reagents initially tested, the positively charged MTSEA (Fig. 2, A and C) or MTSET (Fig. 2 B), were applied either in the continuous presence of glutamate

TABLE I

Positions in NR2C Showing Significant Changes in Leak Current following Exposure to MTSET in the Presence of Coagonists

Position	Δ leak (%)	N	Designation (Fig. 4 A)	Discrete State Dependence
S1-M1/M1				
NR2C(E530)	−77 ± 10%	5	Red	No
NR2C(S533)	−40 ± 6%	4	Red	No
M3/M3-S2				
NR2C(A+3)	−105 ± 14%	5	Red	Yes
NR2C(N+4)	−30 ± 3%	5	Red	Yes
NR2C(A+6)	−367 ± 25%	4	Red	Yes
NR2C(A+7)	−40 ± 3%	5	Red	Yes
S2-M4/M4				
NR2C(D792)	−24 ± 3%	5	Red	No
NR2C(I793)	−55 ± 1%	4	Red	No
NR2C(N795)	+38 ± 4%	4	Black	Yes

Listed are mutant channels, containing cysteine substitutions in the NR2C subunit, where the change in the leak current (Δ leak) following MTSET applied in the presence of coagonists was significantly different from that in wild-type channels (Δ leak = −2 ± 2%, $n = 7$). All mutant channels shown in Fig. 2 were included in this analysis. Values shown are mean ± SEM.

and glycine (Fig. 2, A and B) or in the absence of coagonists but in the presence of the competitive NMDAR antagonist APV (100 μM, open box), which binds to the glutamate binding site on the NR2 subunit, to minimize the probability of channel openings (Fig. 2 C). For wild-type NR1-NR2C channels, I_{post} was unchanged compared with I_{pre}, indicating that possible modifications of endogenous cysteines do not affect current amplitudes. Similarly, a number of cysteine-substituted channels did not show changes in glutamate-activated current amplitude after the MTS application. Others, however, showed either inhibition (Fig. 2 B) or potentiation (Fig. 2 C) of glutamate-activated current amplitudes. In addition, a small subset of cysteine-substituted channels showed a significant change in the holding or leak current following the MTS application in the presence of coagonists (Fig. 2 C; Table I).

Fig. 2 D summarizes the mean percent change (% change) in the amplitude of glutamate-activated currents in NMDAR channels with cysteine substitutions in and around the M1, M3, and M4 segments of the NR2C subunit. These measurements were made before and after exposure to MTSEA (MTSEA + Glu) or MTSET (MTSET + Glu) in the presence of coagonists or to MTSEA in the absence of coagonists but in the presence of APV (MTSEA − Glu). Filled bars indicate positions where % change was significantly different from zero. Based on the assumptions of SCAM (see Discussion), we considered such positions accessible to MTS reagents and exposed to the water interface. Given that one turn of an α-helix contains 3.6 residues and assuming an α-helical structure for transmembrane domains, we also considered four or more consecutive nonaccessible positions on the cytoplasmic side of a tested domain as no longer exposed to the outer cavity and located too deep in the pore to be reached by the externally applied MTS reagents. Fig. 2 D, therefore, shows that, similar to the homologous domains in NR1 (Beck et al., 1999), regions encompassing the N-terminal parts of M1 and M4 and the C-terminal part of M3 in the NR2C subunit contribute to the outer cavity of the NMDAR channel. Notable here in terms of the presumed transmembrane segments (highlighted in gray), only the M3 segment shows an extensive accessibility, as in NR1. Therefore, the NR1 and NR2 subunits make an overall similar contribution to channel structure. As explored in more detail below, however, the accessibility pattern for the two subunits is different, suggesting a subunit-specific contribution to pore structure. Initially, we compared features of accessibility in the presence of the coagonists, glutamate and glycine.

Accessible Positions in the NR2C M1 and M4 Are Located Superficially

One approach to compare the relative location of accessible positions is to measure the rate of modification of substituted cysteines by MTS reagents as a function of membrane potential. A number of factors can influence the voltage dependence of modification rates, including the coupling of the movement of MTS reagents to permeant ions and the local environment. However, we assume that the major factor determining the voltage dependence of modification rates is the relative positioning of substituted residues within the transmembrane electric field. Fig. 3 A illustrates our protocol to measure modification rates in the presence of coagonists. MTSET was applied five times for 1 min in the presence of coagonists (Fig. 3 A) at a holding potential, V_h, of −60 mV. Glutamate-activated current amplitudes, plotted as a function of the cumulative time of MTSET exposure, were fit with a single exponential. The time constant of these fits defined the apparent second order rate constant for chemical modification in the presence of agonists, k. To measure the voltage dependence of modification rates, we performed experiments as in Fig. 3 A at different V_h. Fig. 3 B shows the modification rate constant for NR1-NR2C(A527C), expressed in a logarithmic form $(-(RT/F)*\ln k)$, as a function of V_h. The slope of the fitted line to this plot gave an estimation of $z\delta$, the fraction of the transmembrane electric field the MTS reagent passes to reach the exposed cysteine (δ) multiplied by the reagent charge (z) (see Materials and Methods). For NR1-NR2C(A527C), $z\delta$ was close to zero ($z\delta = -0.01 \pm 0.02$) (mean ± SEM), indicating that the rate was voltage independent.

Fig. 3 C summarizes modification rates at −60 mV (left panel) and their voltage dependence (right panel) for selected positions in NR2C. No apparent voltage dependence was observed for any of the tested positions

in NR2C M1 or M4. In contrast, L544C in M1 of NR1 (position homologous to voltage-independent position A527C in NR2C) showed a small but robust voltage dependence (see Sobolevsky et al., 2002b). Further, positions in the M3 segments showed a strong voltage dependence with that for the presumed deepest accessible positions ($z\delta \approx 0.71$ for NR1(V-2C)-NR2C and $z\delta \approx 0.69$ for NR1-NR2C(V-5C)) comparable to that for the N sites in the M2 loop ($z\delta \approx 0.65$ for NR1(N598C)-NR2C and $z\delta \approx 0.72$ for NR1-NR2C(N593C)). These results are consistent with the idea that the M3 segments from the two subunits form the deepest part of the outer cavity, specifically that part directly leading up to the channel's narrow constriction and that regions N terminal to M1 and M4 and C terminal to M3 contribute to more superficial portions of the outer cavity, including the external entrance as well as possibly side entrances to the central cavity at the level of the channel-LBD linkers.

Homologous Domains in the NR1 and NR2C Subunits Show Differences in Surface Exposure

To initially contrast the contribution of regions in and around the NR1 and NR2C transmembrane segments to the NMDAR channel, we represented the results of steady-state accessibility experiments illustrated in Fig. 2 in a discrete fashion distinguishing three different types of effects that MTS reagents produced on glutamate-activated currents: (1) inhibition (% change > 0, black positions), (2) potentiation (% change < 0, red positions), and (3) no effect (noncolored positions). This representation gives only a rough outline of the contribution and general orientation of domains to the ion channel pore. Indeed, steady-state experiments, where high concentrations of MTS reagents (2 mM) are applied to cysteine-substituted channels for fairly long periods of time are useful in defining general water accessibility but certainly can give false positives (especially in the case of MTSEA, which can exist in a membrane-permeant form) and/or can identify as water-accessible positions that might only extremely rarely visit such an environment.

Fig. 4 A shows the discrete steady-state accessibility of substituted cysteines in the presence of coagonists on helical nets. We assume that the secondary structure of common regions between subunits is comparable, most likely being α-helical for the transmembrane segments (gray regions in helical nets). Since positions in the linker regions (S1-M1, M3-S2, and S2-M4) react with MTS reagents in a voltage-independent manner, they are presumably located outside the transmembrane electric field. The accessibility pattern for these positions therefore may not show an α-helical pattern (three to four residue periodicity) either because they have a nonhelical secondary structure or have water accessibility on all sides of an α-helix. Nevertheless, since we are mainly interested in similarities and differences between homologous regions in NR1 and NR2C, this approach permits a relative comparison of them.

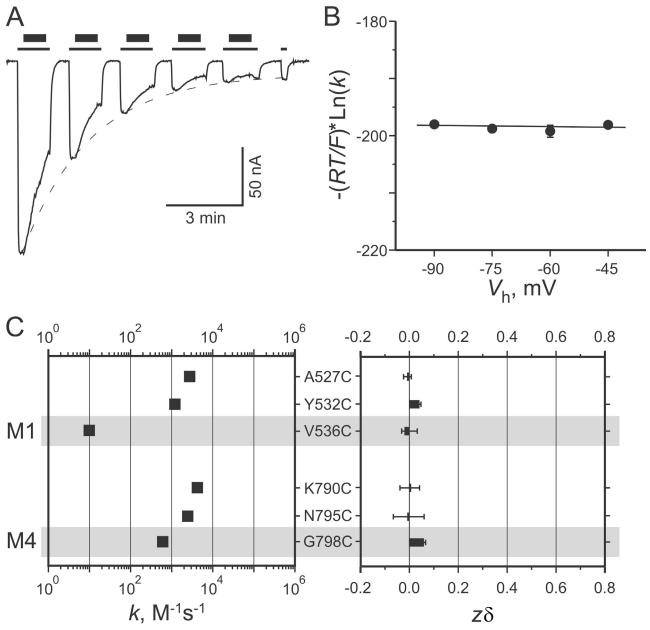

Figure 3. Voltage dependence of the modification rates of exposed cysteines in the presence of agonists. (A) Pulsive protocol to assay modification rates of exposed cysteines in the presence of glutamate/glycine. The example shows NR1-NR2C(A527C) channels. V_h was −60 mV. The MTSET application (4 μM, thick line, 1 min) was started 15 s after the beginning and finished 15 s before the end of the glutamate/glycine (thin line) application. The cell was washed for 1 min between agonist applications. Current amplitudes, defining the time course of cysteine modification, were measured during the first 15 s of each glutamate exposure. Single exponential fit of these current amplitudes as a function of cumulative time of MTSET exposure (dashed line) gives the time constant $\tau = 78 \pm 2$ s. The corresponding rate constant of chemical modification in the presence of agonists, k, was 3205 ± 82 $M^{-1}s^{-1}$. (B) Apparent second-order rate constant for chemical modification of NR1-NR2C(A527C) by MTSET in the presence of agonists, expressed in a logarithmic form ($-(RT/F)*\ln k$), as a function of the holding membrane potential, V_h. The k values were estimated using the protocol illustrated in A. The error bars are not shown if smaller than the symbol size. The straight line through the points is a fit with Eq. 2 (see Materials and Methods). The slope of this fit gives $z\delta = -0.01 \pm 0.02$. (C) Mean values of k at $V_h = -60$ mV and $z\delta$ for selected positions in NR2C. Rate constants for substituted cysteine modification were measured for MTSET (squares). SEMs are smaller than the symbol size ($n > 4$). Positions that belong to the M1 or M4 segments are highlighted in gray.

To compare surface exposure of different regions, we grouped neighboring black and red positions into clusters. A neighboring position is one of the six positions surrounding a selected one on the surface of an α-helix: two positions, the preceding and following ones in the polypeptide chain, that belong to the same turn of the α-helix, and the four closest positions in the turn below (two positions) and in the turn above (two positions).

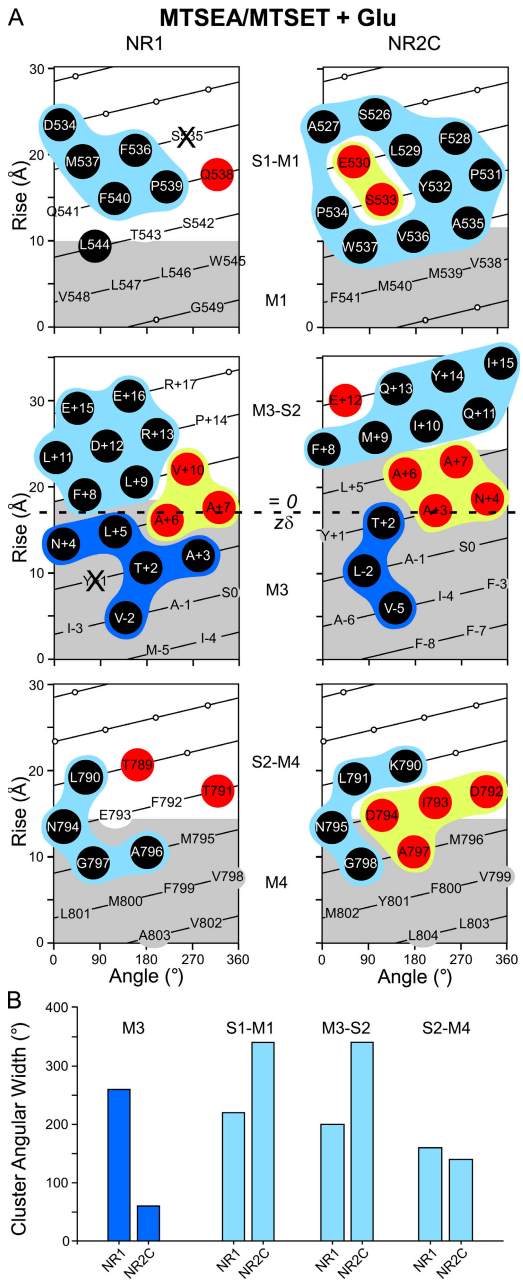

Figure 4. Analysis of substituted cysteine reactivity with MTSEA/MTSET in the presence of glutamate/glycine. (A) Helical net diagrams illustrating discrete reactivity of substituted cysteines in and around the M1 (top row), M3 (middle row), or M4 (bottom row) segments of NR1 (left half) and NR2C (right half) subunits with MTS reagents in the presence of agonists (MTSEA/MTSET+Glu). All positions indicated were tested for accessibility. Mutants that did not generate detectable glutamate-activated currents are indicated with an X (NR1(S535C)-NR2C and NR1(Y+1)-NR2C). MTSEA and/or MTSET either inhibited (black circles), potentiated (red circles), or had no effect (no circle) on glutamate-activated currents. The data for NR1 are from Beck et al. (1999) and Watanabe et al. (2002), and that for positions W613C-I633C (F-8 to I+10) in NR2C M3 are from Sobolevsky et al. (2002b). Gray regions denote the hydrophobic segments (M1, M3, and M4) (see Fig. 1 B). We aligned positions in M1 and M3 according to their voltage dependence (Fig. 3) (Sobolevsky et al., 2002b). The dashed line in M3s indicates the approximate boundary between positions with voltage-dependent and -independent reaction rates. Positions in M4 did not show any notable voltage dependence so we aligned them according to sequence homology. Clusters of positions with similar properties are highlighted in light blue (black positions with voltage-independent modification rates), dark blue (black positions with voltage-dependent modification rates), and yellow (red positions). (B) Angular width (see Materials and Methods) of dark and light blue clusters of positions that presumably face the ion conduction pathway.

We define a cluster as a continuous group of neighboring positions with common functional properties. For example, clusters of black positions with % change > 0 are highlighted in blue, whereas clusters of red positions with % change < 0 are highlighted in yellow. The voltage dependence of modification rates (Fig. 3) represents an additional functional property that distinguishes clusters with % change > 0 into voltage dependent (dark blue) and voltage independent (light blue).

Fig. 4 A shows that most black and red positions can be grouped into clusters. Notably, red positions (yellow clusters) do not appear to be randomly distributed on the surfaces of presumed α helices. Even in the two regions where there are no yellow clusters (NR1 S1-M1 and NR1 S2-M4), the single red position in NR1 S1-M1 (Q538) has a neighbor (S535) that generates nonfunctional channels, whereas in the case of NR1 S2-M4, the two red positions could form a cluster but data are not available for a potential common neighbor, position 788. In any case, this clustering of red positions, a result most notable for the M3 segments, suggests that they share a common structural property. As discussed further below, we propose that red positions are preferentially located at protein–protein or protein–lipid interfaces. Accordingly, blue clusters represent surfaces of the protein that preferentially face the ion conducting pathway or central pore that encompass, for the outer cavity, the central cavity itself as well as the side entrances leading up to it. We will initially contrast the contribution of blue clusters of the two subunits to the channel pore and then return to red positions in subsequent figures.

To compare the contribution of NR1 and NR2C subunits to the pore-lining surface, we measured the angular width of each blue cluster, which is defined as the angular size of the smallest sector that is covered by this cluster on the surface of the corresponding α-helix (Fig. 4 B; see Materials and Methods). The M3 segments in both NR1 and NR2C contribute to the deep (voltage dependent) portion of the outer cavity (dark blue clusters) but the contribution of NR1 M3 (260°) is greater than that of NR2C M3 (60°) (Fig. 4 B). Complimentary, NR2C makes a greater contribution to the shallow (voltage independent) portion of the outer cavity (light blue clusters) with more residues in pre-M1 (340°) and M3-S2 linker (340°) of NR2C compared with pre-M1 (220°) and M3-S2 linker (200°) of NR1 facing the central pore.

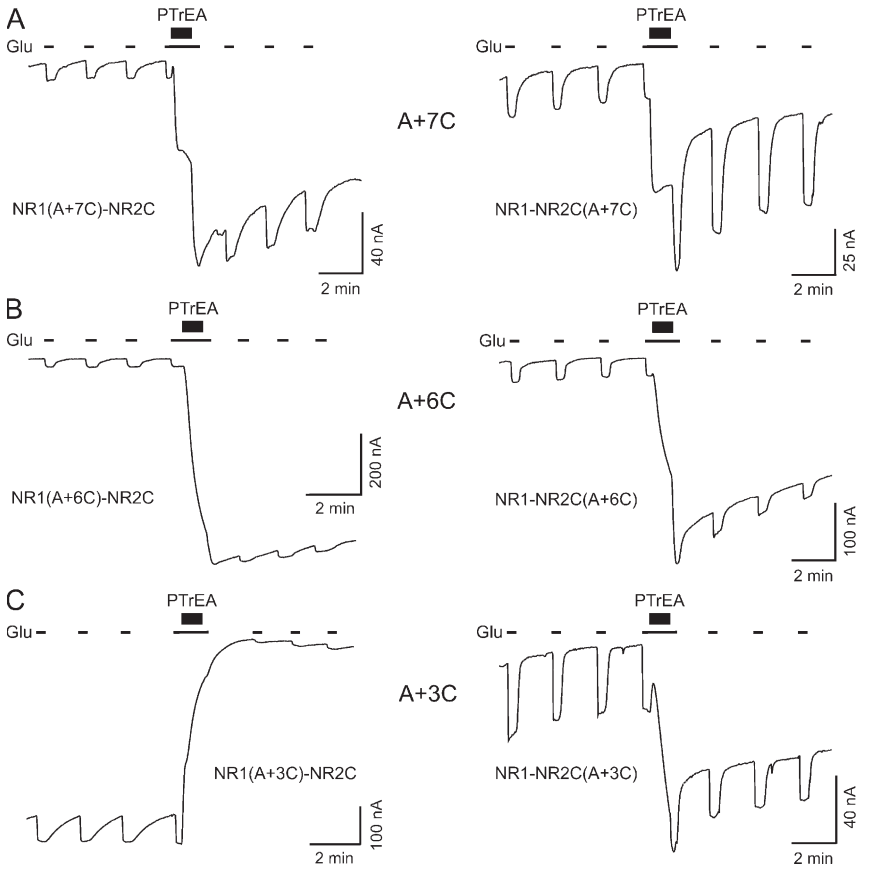

Figure 5. Effect of the large-sized MTS reagent PTrEA applied in the presence of glutamate/glycine on alanine-to-cysteine substitutions in SYTANLAAF. (A–C) Example recordings showing the effect of the MTS reagent PTrEA on substituted cysteines in the NR1 (left) or NR2C (right) M3 segments. PTrEA was applied in the presence of glutamate/glycine (thin lines) (see Fig. 2). Homologous positions are aligned horizontally.

The M4 segments and S2-M4 linkers in NR1 and NR2C subunits make relatively small and nearly identical (160° and 140°, respectively) contributions. The large angular widths calculated for some of the light blue (voltage independent) clusters may reflect (see also Discussion) (a) a nonhelical secondary structure, (b) an α-helix that may be in contact with both the central cavity as well as side entrances to it, and/or (c) dynamic nature of the corresponding regions.

One notable difference between the M3 segments is the lack of accessibility for NR2C(L+5), which breaks the connectivity of the blue clusters. This position is unlikely to be silent since neither MTSEA, MTSET (Fig. 2 D), nor PTrEA (see Fig. 6 A) alter current amplitudes for L+5C. In addition, application of DTT (unpublished data) to this mutant has effects comparable to wild type, suggesting that cysteines introduced at L+5 for two NR2C subunits do not spontaneously cross-link. Hence, in contrast to NR1, the L+5 position in NR2C is not accessible, supporting the overall difference in contribution of the NR1 and NR2C M3 segments to pore structure.

The above analysis suggests an unequal contribution of homologous domains in the NMDAR subunits to pore structure. Because M3 is the only transmembrane segment that contributes to the deep (voltage dependent) portion of the outer cavity, placing more constraints on its accessibility, we focused mainly on M3 to further explore this unequal contribution and to clarify more fully the properties of red positions.

Differential Access of the NR1 and NR2C M3 Segments to the Large-sized MTS Reagent PTrEA

Initially, we compared the accessibility of substituted cysteines in the M3 segments between NR1 and NR2C subunits to the large-sized MTS reagent PTrEA. We anticipate that if there is a differential positioning of the M3 segments relative to the central axis of the pore, these differences would become more pronounced with this larger-sized MTS reagent. We also considered in detail the effect of PTrEA not only on glutamate-activated currents but also on leak currents.

Fig. 5 (A–C) illustrates the effect of PTrEA applied in the presence of glutamate/glycine on mutant channels containing cysteine substitutions of alanines in the highly conserved SYTANLAAF motif. The majority of these alanines (A+6 and A+7 in NR1 as well as all in NR2C) are demarcated as red in Fig. 4 A. In the case of A+7 (Fig. 5 A) and A+6 (Fig. 5 B), glutamate-activated and leak currents displayed similar phenotypes for the NR1 and NR2C subunits following the PTrEA application. Indeed, glutamate-activated current amplitudes were strongly potentiated (A+7, % change < -100) or weakly inhibited (A+6, % change > 0), while in both instances

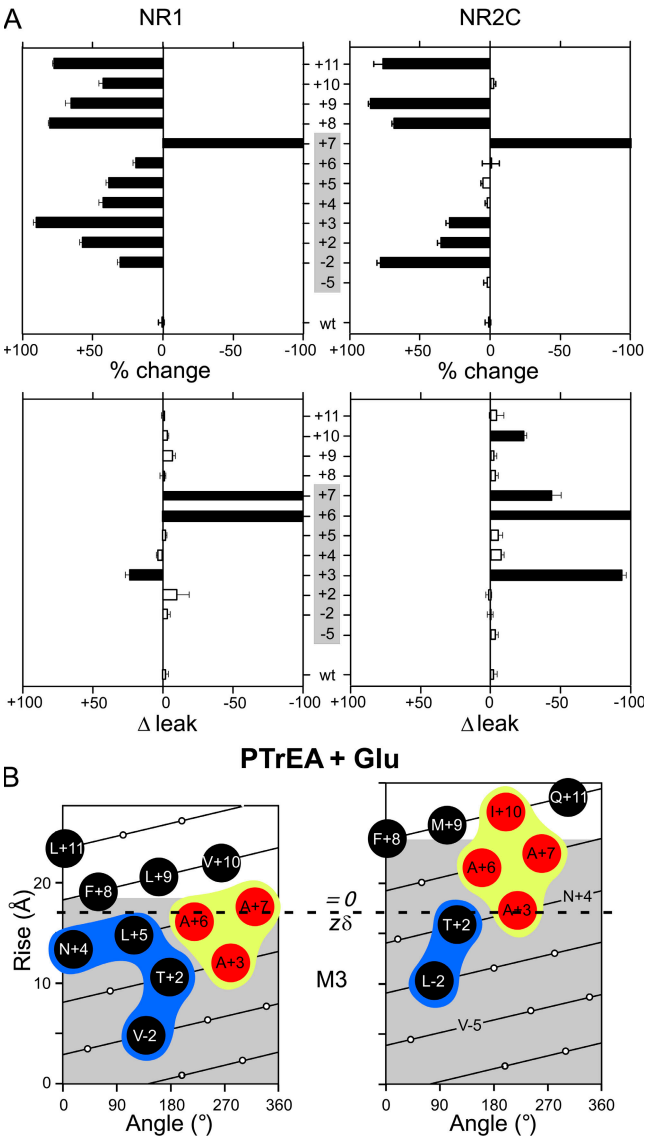

Figure 6. Accessibility of substituted cysteines in the NR1 and NR2C M3 segments to PTrEA applied in the presence of glutamate/glycine. (A) Mean percent change (% change) in glutamate-activated current amplitudes (first row) or in leak currents (Δ leak) (second row) measured before and after exposure to PTrEA in the presence of glutamate/glycine. Left and right pointing bars indicate inhibition and potentiation, respectively ($n > 4$). For positions with % change = −100 or Δ leak = −100, potentiation was stronger than 100%. Filled bars indicate that the value of % change or Δ leak is statistically different from zero. (B) Helical net analysis of the NR1 and NR2C M3 segments showing discrete accessibility to PTrEA in the presence of glutamate/glycine (PTrEA+Glu). All positions indicated were tested for accessibility to PTrEA. The display is comparable to that in Fig. 4 but expands the definition of red positions to include those that show a significant change in leak current.

leak currents were strongly increased (Δ leak < 0). The change in leak current was most notable for A+6 (Δ leak = −320 ± 80%, $n = 5$, for NR1(A+6C)-NR2C and Δ leak = −300 ± 10%, $n = 7$, for NR1-NR2C(A+6C)), consistent with previously published results (Jones et al., 2002; Yuan et al., 2005). In addition, a significant increase in leak current, albeit smaller in magnitude, was also observed for NR1 and NR2C A+7 positions (Δ leak = −150 ± 20%, $n = 6$, and Δ leak = −40 ± 7%, $n = 5$, respectively).

In contrast to A+7 and A+6, leak currents for cysteine substitutions at A+3 in NR1 and NR2C showed qualitatively different phenotypes following the PTrEA application (Fig. 5 C). Indeed, although glutamate-activated currents were inhibited in both instances, with a somewhat stronger effect occurring for NR1 A+3, leak currents changed in opposite directions, being significantly decreased for NR1(A+3C)-NR2C (+23 ± 3%, $n = 9$) but increased for NR1-NR2C(A+3C) (−90 ± 3%, $n = 7$). We propose that in the case of NR1(A+3C)-NR2C, the cysteine substitution itself significantly changes channel function (see below).

Fig. 6 A summarizes the effect of PTrEA applied in the presence of glutamate/glycine on glutamate-activated (% change) and leak (Δ leak) currents for cysteines substituted in the M3 segments of NR1 (left) and NR2C (right). These results are further summarized, in a discrete manner (inhibition, potentiation, and no effect), on helical nets in Fig. 6 B. In general, these plots are comparable to those for MTSEA/MTSET (Fig. 4 A) with several exceptions (NR1 A+3 and V+10 and NR2C V-5, N+4, and I+10). Some of the differences reflect that positions in NR2C (V-5 and N+4), which were accessible to MTSEA and/or MTSET, are no longer accessible to PTrEA. Other differences reflect that we have expanded out the definition of red positions to include not only those that show potentiation of glutamate-activated currents but also those with significant changes in leak current (i.e., NR1 A+3 and NR2C I+10) (see below and Table II).

Leak current, which along with other components, can include current through NMDAR channels activated in the absence of added coagonists, is an approximate index of the stability of the closed state. As summarized in Table II, most (six of seven) of the M3 positions that showed potentiation of glutamate-activated currents after application of either MTSEA/MTSET (Fig. 4 A) or PTrEA (Fig. 6 A), also showed significant changes in leak current (see also Jones et al., 2002; Yuan et al., 2005). In addition, although we do not have the data for NR1 positions, which were not published in Beck et al. (1999), a similar relationship was observed for many NR2C positions following MTSET treatment, with 8 out of 11 positions demarcated as red in Fig. 4 A showing a significant change in leak current (Table I). Such a coincidence of potentiation of glutamate-activated currents and changes in leak current for positions in yellow clusters suggests a common basis for an alteration of gating. We therefore propose that potentiation of glutamate-activated currents as well

TABLE II

Properties of Positions Designated as Red in the NR1 and NR2C M3 Segment

Position	% change	Δ leak	Designation (Fig. 4 A)	Designation (Fig. 6 B)	Discrete State Dependence
NR1					
NR1(A+3)	>0 (I)	Yes	Black	Red	No
NR1(A+6)	<0 (P)	Yes	Red	Red	Yes
NR1(A+7)	<0 (P)	Yes	Red	Red	No but $k/k_{APV} > 100$
NR1(V+10)	<0 (P)	No	Red	Black	No
NR2C					
NR2C(A+3)	<0 (P)	Yes	Red	Red	Yes
NR2C(N+4)	<0 (P)	–[a]	Red	–	Yes
NR2C(A+6)	<0 (P)	Yes	Red	Red	Yes
NR2C(A+7)	<0 (P)	Yes	Red	Red	Yes
NR2C(I+10)	>0 (I)	Yes	Black	Red	No

Listed are mutant channels, containing cysteine substitutions in the NR1 or NR2C M3 segment, that were designated red either in Fig. 4 A or Fig. 6 B. For % change, we indicated that it was <0 (potentiation) if this occurred for at least one of the test reagents, MTSEA, MTSET, or PTrEA (see Discussion). Δ leak indicates that there was a significant change in leak current following treatment with PTrEA (Fig. 6 A). A similar quantification was made for MTSET for NR2C (Table I) but not for NR1 positions (Beck et al., 1999).

[a]NR2C(N+4) was not accessible to PTrEA. It was accessible to MTSET and showed a significant change in leak current (Table I).

as changes in leak current reflect that the presence of the bulky side chain following reaction of the MTS reagent destabilizes the closed state (because these positions are located in the vicinity of other protein or lipid elements) and shifts the equilibrium in the presence of coagonists between the closed and open states toward the open state. Consistent with this idea is the observation that many red positions, at least those in the M3 segment, show a strong state dependence, either in terms of discrete accessibility or reaction rates (Table II) (see below).

In summary, the helical nets in Fig. 6 B highlight two general observations. First, they further support the idea that the NR1 M3 segment shows a greater exposure to the central pore than the NR2C M3 (angular width of 160° versus 40° for dark blue clusters). Second, although the NR1 and NR2C M3 segments show differences in terms of their positioning relative to the central and vertical axes of the channel, they share a common overall orientation with comparables sides of presumed α helices facing the central axis of the pore (dark blue clusters). In this interpretation, red positions, which cluster together in both subunits, are located on the back side of the α-helix.

Cysteine Substitution of NR1(A+3) Itself Alters Channel Function

In oocytes injected with NR1(A+3C)-NR2C mRNA, PTrEA significantly reduces leak current (Fig. 5 C), a phenotype unique to this position (Fig. 6 A). We interpreted this result as if the cysteine substitution itself significantly changes channel function and that some portion of the leak current is carried by NR1(A+3C)-NR2C channels active even in the absence of applied agonists. To test this idea, we studied the effect of Mg^{2+}, a well-known pore blocker of NMDAR channels, on leak and glutamate-activated currents in NR1-NR2C channels carrying single cysteine substitutions of alanines in SYTANLAAF (Fig. 7).

Extracellular Mg^{2+} (100 μM) had only small effects on current amplitudes in oocytes injected with wild-type NR1-NR2C (Fig. 7 A) when applied in the absence of agonists (initial application) (Δ leak = 1 ± 1%) but strongly reduced currents in the presence of agonists (second application) (% change = 33 ± 1%). In contrast, in oocytes injected with NR1(A+3C)-NR2C (Fig. 7 B), Mg^{2+} produced a much greater inhibition of current amplitudes both in the absence (Δ leak = 20 ± 2%) and presence (% change >100%) of agonists. As summarized in Fig. 7 C, the cysteine substitution of A+3 in NR1 was the only one to show a significant effect of Mg^{2+} on leak current. These results are consistent with the idea that the cysteine substitution of NR1 A+3 itself alters channel function, yielding channel activity even in the absence of applied agonists. Such effects were observed for certain substitutions at the Lurcher position (A+7) (Kohda et al., 2000; Taverna et al., 2000) or T+2 in NR1 (Kashiwagi et al., 2002) and could be due to channels that (a) are constitutively open and/or (b) have increased agonist affinity/reduced desensitization and, as a result, can be activated by ambient concentrations of agonists (Klein and Howe, 2004).

State Dependence of Accessible Surfaces Represented by NR1 and NR2C Subunits

Fig. 8 A illustrates accessibility of regions in and around the transmembrane segments in NMDAR subunits in the absence of agonists shown in Fig. 2. These results are again represented in a discrete fashion distinguishing three different types of effects that MTS reagents

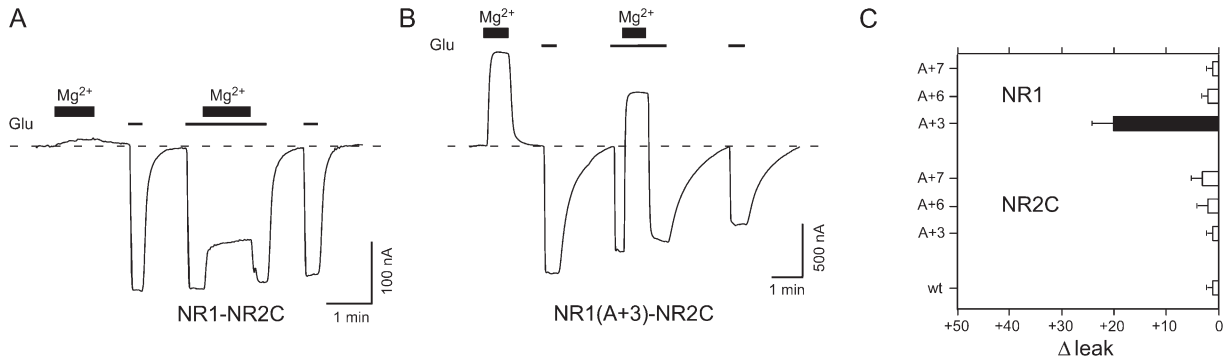

Figure 7. Mg^{2+} block of leak and glutamate-activated currents. (A and B) Example recordings showing the effect of extracellular Mg^{2+} (100 μM, thick lines) on leak (initial application) or on glutamate-activated (second application) currents in oocytes injected with wild-type NR1-NR2C (A) or NR1(A+3C)-NR2C (B) mRNA. Thin lines indicate applications of glutamate/glycine. V_h was −60 mV. (B) Mean percent change in leak currents (Δ leak) upon application of extracellular Mg^{2+} ($n > 4$). A filled bar indicates that the value of Δ leak is statistically different from zero.

produced on glutamate-activated currents: (1) inhibition (% change > 0, black positions), (2) potentiation (% change < 0, red positions), and (3) no effect (non-colored positions). As in Fig. 4, we do not consider leak current in our definition of red positions here since comparable data was not published for NR1 positions.

Contrasting the regions in and around M1 and M4 in Fig. 4 A and Fig. 8 A, only one position in NR1 (L544 in M1; Beck et al., 1999) and one in NR2C (V536 in M1; Fig. 2) showed discrete state dependence. On the other hand, the largest number ($n = 5$) of state-dependent positions was found in the NR2C M3 segment (V-5, A+3, N+4, A+6, and A+7). The NR1 M3 segment had a smaller number of state-dependent positions ($n = 2$). Here, A+6 showed reactivity in the presence of agonists but did not show it in the absence of agonists (unpublished data) (Jones et al., 2002; Yuan et al., 2005). On the other hand, A+3 did show reactivity in the absence of agonists (Beck et al., 1999), but this most likely reflects that these channels are active even in the absence of added agonists (see Fig. 7). Hence, in homology to NR2C, we classified A+3 as not accessible in the absence of glutamate.

Fig. 8 B contrasts the angular width for the dark blue and yellow clusters in the NR1 and NR2C M3 segments in the presence and absence of glutamate/glycine. Clearly, the dark blue clusters show a significant change in surface coverage, being reduced from 260° to 160° (a 38% decrease) for NR1 M3 and from 60° to 40° (a 33% decrease) for NR2C M3. On the other hand, a more drastic reduction in coverage was observed for the yellow clusters, being reduced from 100° to 60° (a 40% decrease) for NR1 and from 160° to 0° (a 100% decrease) for NR2C. In general, these results are consistent with the idea that the red positions do not face the water-filled pore in the absence of glutamate.

Although the NR1 M3 segment shows a limited discrete state dependence, reactivity of these substituted cysteines with MTS reagents based on the more sensitive reaction rates is in fact strongly state dependent (Sobolevsky et al., 2002a). The reason we do not see a more extensive discrete state dependence in NR1 M3 is that, despite differences in the rates of modification in the presence and absence of agonists, these rates even in the absence of agonist are much faster than 1 $M^{-1}s^{-1}$, the limit of resolution for our kinetic experiments (see Materials and methods). Therefore, to uncover possible state dependence and to further compare the relative role of different NR1 and NR2C regions to gating, we measured the modification rate of substituted cysteines in the absence of glutamate/glycine.

State-dependent Modification Rates of Cysteine-substituted NMDAR Channels

Fig. 9 A illustrates our protocol to measure modification rates in the absence of glutamate and glycine. MTSET was applied five times for 1 min in the absence of coagonists but in the presence of APV at a holding potential of −60 mV. Glutamate-activated current amplitudes, plotted as a function of the cumulative time of MTSET exposure, were fit with a single exponential. The time constant of these fits defined the apparent second order rate constant for chemical modification in the absence of agonists, k_{APV}.

The difference between k and k_{APV} in general was greatest for the M3 segments (Fig. 9 B, right), where 9 out of 13 positions tested showed at least a 10-fold difference in k_{APV} compared with k. In addition, similar values of k/k_{APV} for vertically aligned positions in NR1 and NR2C indicate that their M3 segments experience comparable state-dependent changes in accessibility. We used different size MTS reagents for measuring the modification rates of substituted cysteines. Given that the specific reagent (MTSEA, MTSET, and PTrEA) may strongly affect reaction rates, this may complicate a comparison across reagents. However, since the M3 segments

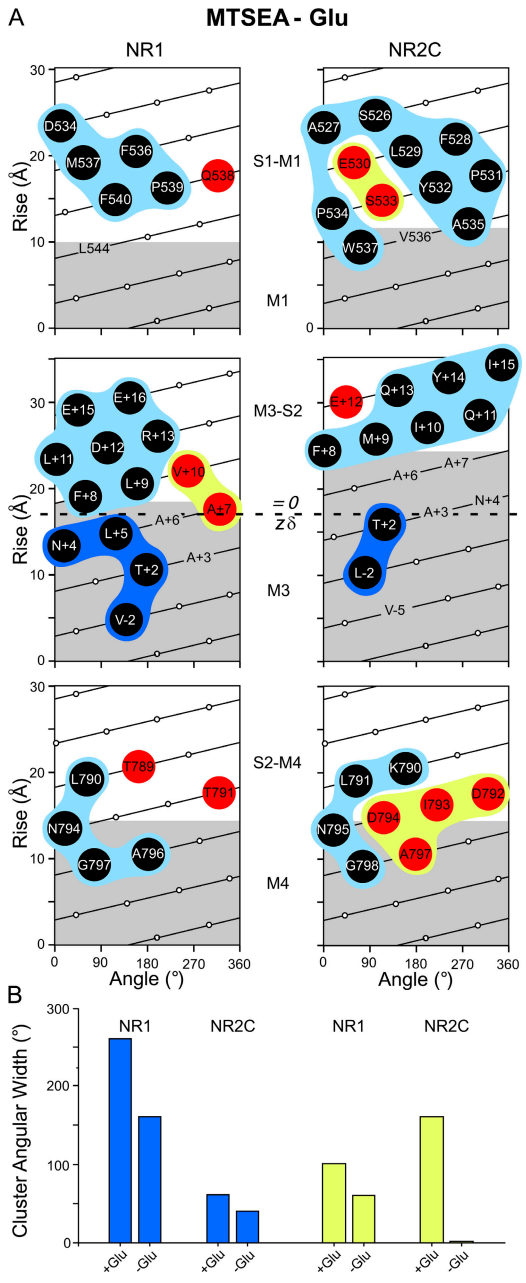

Figure 8. Analysis of substituted cysteine reactivity with MTSEA in the absence of glutamate/glycine. (A) Helical net diagrams illustrating discrete reactivity of substituted cysteines in and around the M1 (top row), M3 (middle row), or M4 (bottom row) segments of NR1 (left) and NR2C (right) subunits with MTSEA in the absence of agonists (MTSEA-Glu). The data for NR1 are from Beck et al. (1999), whereas that for NR2C is from Fig. 2 D. Within each helical net the gray region denotes the hydrophobic segment. Only positions reactive in the presence of coagonists (Fig. 4 A) are indicated. The results shown are for steady-state reactions for MTSEA with two exceptions. Positions S452 and T543 in NR1 S1-M1 are accessible in the absence but not in the presence of glutamate (Beck et al., 1999). However, this effect was only marginally statistically significant and it seems highly unlikely that there would be positions accessible in the absence of glutamate (closed state) but not also accessible in the presence of glutamate (closed and open states). We therefore for simplicity did not indicate that these positions were accessible in the absence of glutamate.

in both subunits were probed with multiple reagents and they intertwine throughout the entire length of this segment showing consistent changes in both k/k_{APV} (Fig. 9 B) and $z\delta$ (Sobolevsky et al., 2002a,b), we believe that the type of the MTS reagent used does not change our major conclusions. Therefore, the difference in discrete state dependence observed for M3 between NR1 and NR2C (Fig. 2 D and Fig. 8) presumably is the result of the overall faster reaction rate for cysteines substituted in NR1 than in NR2C. For example, the rate of modification by MTSEA for positions V-2 and T+2 in NR1 was faster than that for V-5 and L-2 as well as T+2 in NR2C (Fig. 9 B, left). On the other hand, the modification rates for pre-M1/M1 were less state dependent than those for M3 with only three out of six positions tested showing at least a 10-fold difference in k/k_{APV}. The smallest state dependence in modification rates was observed for pre-M4/M4 where only one out of six positions showed at least a 10-fold difference in k/k_{APV}.

In summary, the large difference between modification rates measured in the presence and absence of agonists for the M3 segments in both NR1 and NR2C subunits supports the idea that, at least relative to the other regions studied here, they are strongly involved in gating. Smaller difference between k and k_{APV} for M1 and almost no difference for M4 most likely reflect gradually smaller contribution of these regions to gating.

DISCUSSION

We used the substituted cysteine accessibility method (SCAM) and channel block to contrast the contribution of NMDAR subunits to channel structure and gating. The interpretation of our results is limited by the assumptions of SCAM (Karlin and Akabas, 1998). For example, we assume that the cysteine substitution itself does not significantly alter the conformation of the protein, though in at least one instance it apparently does (Figs. 5–7). We also consider a substituted cysteine to be exposed to the water interface if glutamate-activated currents are persistently altered following the application of an MTS reagent. We assume that a lack of a persistent effect on glutamate-activated currents reflects that the substituted cysteine is not in a water interface, presumably because it is buried in the interior of the protein or faces membrane lipids. In certain instances, exposed cysteines may not be modified or may be modified

Positions K790 and N795 do not show reactivity with MTSEA either in the presence or absence of glutamate (Fig. 2 D) but do show a robust reactivity with MTSET both in the presence and absence of glutamate (Fig. 2 D and Fig. 9 B, respectively). The lack of an effect with MTSEA presumably reflects a silent reaction, an action we do not explore further here. (B) Angular width of the NR1 and NR2C M3 dark blue and yellow clusters in the presence (+Glu) or absence (−Glu) of glutamate/glycine.

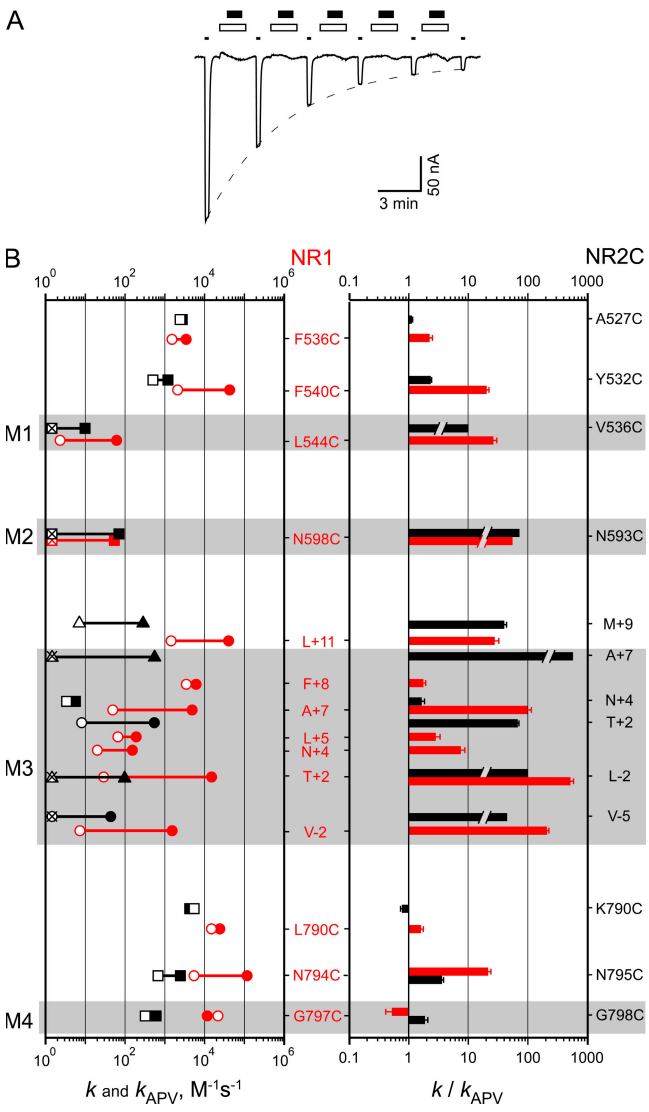

Figure 9. Modification rates of exposed cysteines in the absence of glutamate. (A) Pulsive protocol to assay modification rates of exposed cysteines in the absence of glutamate. The example shows NR1-NR2C(A527C) channels (as in Fig. 3 A). V_h was −60 mV. 1 min after a 15-s test glutamate application (thin line), APV (100 µM, open box) was applied for 1.5 min. The MTSET application (5 µM, thick line, 1 min) was started 15 s after the beginning and finished 15 s before the end of the APV exposure. After APV, the cell was washed for 1.25 min before the next test glutamate application. Dashed line illustrates a single exponential fit of the current amplitudes as a function of cumulative time of MTSET exposure ($\tau = 93 \pm 3$ s) that defines the rate constant of chemical modification in the absence of glutamate, k_{APV}, which was 2151 ± 70 $M^{-1}s^{-1}$. (B) Mean values of k (solid symbols), k_{APV} (open symbols), and k/k_{APV} (columns) at $V_h = -60$ mV for NR1 (red) and NR2C (black) subunits (values for k are from Fig. 3 C). Rate constants for substituted cysteine modification were measured for MTSEA (circles), MTSET (squares), or PTrEA (triangles). SEMs are smaller than the symbol size ($n > 4$). Crossed symbols represent the k_{APV} values smaller than 1 $M^{-1}s^{-1}$. Cut bars on the right plot indicate that the corresponding k/k_{APV} values are larger than shown since in these instances $k_{APV} \leq 1$ $M^{-1}s^{-1}$. The data for NR1 positions are from Sobolevsky et al. (2002a). For the NR2C M3 segment, the k values are from Sobolevsky et al. (2002b). Positions that belong to the M1, M2, M3, or M4 segments are highlighted in gray.

without producing a persistent effect (silent reaction). Sometimes, to maximize the absolute value of the effect, we used MTSEA, which can exist in a nonionized form, as a test reagent. However, in the majority of our experiments, we used the permanently charged reagents MTSET and PTrEA, and the results of these experiments are consistent with the results for MTSEA (with the exception of two positions in the M3-S2 linker). Taking into account the limitations and assumptions of SCAM, our experiments can provide only low-resolution information about the structure and gating of the NMDAR channel. Nevertheless, this information is invaluable in terms of defining the general arrangement of pore-forming domains and will be extremely useful when structures of full-length GluRs are solved.

Distinction into Black and Red Positions

Although we followed the basic assumptions of SCAM and typically looked only at binary effects, we distinguished positions that showed a significant effect on NMDAR-mediated currents into black (% change > 0) and red (% change < 0). Although we do not know the detailed basis for inhibition and potentiation—and they may not all have a common basis—we suggest as a first approximation the following conditions. In both the open and closed states, black positions typically face the central or most water-exposed portion of the pore, including the central cavity as well as the side entrances at the level of channel-LBD linkers leading up to it. In contrast, red positions are preferentially, at least in the closed state, remote from the central axis of the pore, being located at protein–protein or protein–lipid interfaces. Accordingly, we assume that red positions are transiently placed in the vicinity of the central axis of the pore in the open state of the channel and/or that MTS reagents interact with these red positions remote from the central pore (e.g., via crevices or interlinker pores). We therefore propose that potentiation of glutamate-activated currents reflects that the presence of the bulky side chain following reaction of the MTS reagent destabilizes the closed state (because these positions are in the vicinity of other protein or lipid elements) and shifts the equilibrium in the presence of coagonists between the closed and open states toward the open state. Several lines of evidence support this idea. First, red positions tend to cluster together (Fig. 4 A) as if they share common structural properties. Further, leak current, which is an approximate index of the stability of the closed state in the absence of agonists, is also typically increased for red positions following MTS application. For the M3 segments, where we have such data for both the NR1 and NR2C subunits, six out of seven positions show such a strict relationship (Table II) (see also Jones et al., 2002; Yuan et al., 2005). In addition, NR1(A+3) shows inhibition of glutamate-activated currents (classified as black in Fig. 4 A), and a significant change in leak

current (Fig. 6 A). This phenotype is not inconsistent with the overall hypothesis since the significant change in leak current was a decrease not an increase, and the cysteine substitution itself at this position disrupted channel function. Similarly for the NR2C subunit (comparable data was not published for the NR1 subunit), 8 of the 11 positions classified as red in Fig. 4 A showed significant changes in leak current, whereas only 1 of the 24 positions designated as black did so (Table I). Also consistent with the general hypothesis is the observation that most positions classified as red, at least in M3, also showed a strong state dependence, either in terms of discrete state dependence or reaction rates, as if these positions are located remote from the water-accessible surface in the closed state (Fig. 8 A and Fig. 9 B).

In some instances, certain positions showed mixed properties (inhibition or potentiation) depending on which reagent was used (MTSEA, MTSET, and/or PTrEA) (e.g., NR2C(A+6), NR2C(A+7), and NR2C(N795)). Although we do not fully understand all of the molecular details underlying these effects, a number of different factors could come into play, including the size of the reagent, the number of cysteines modified (two, one in each of two identical subunits, have been introduced), the local spatial constraints around the introduced cysteine, and the overall energy difference between activation states. One could envision that some interplay of all of these factors could determine the sign of change of glutamate-activated or leak currents. Although our approach might certainly misclassify certain positions, we believe that our overall conclusions, drawn from patterns rather then individual results for selected positions, are correct.

Differential Contribution of Homologous Domains in NR1 and NR2C Subunits to Pore Structure

Based on the results of present and previous studies, we propose that homologous domains in NMDAR subunits contribute differently to pore structure at various levels of the channel. We divide the outer cavity of the NMDAR channel into two different regions: deep, where the transmembrane voltage drops, and shallow, where the interaction of substituted cysteines with positively charged MTS probes is voltage independent (Fig. 3).

The pore-lining surface of the deep portion of the outer cavity is formed exclusively by the M3 segments from the NR1 and NR2C subunits (deep blue clusters in Fig. 4 A). Indeed, for both NR1 and NR2C, only a limited number of positions were accessible in the M1 and M4 segments. In addition, with one exception [NR1(L544C)], the modification rate of substituted cysteines in and around M1 and M4 are voltage independent (Fig. 3) (Sobolevsky et al., 2002a).

Although the NR1 and NR2C M3 segments both contribute to lining the deep portion of the outer cavity, they do not appear to do so equally. In particular, the angular width of the dark blue cluster, which we assume represents the side of the helix facing the central pore, is much larger for the NR1 M3 segment than that for the NR2C M3 segment both in the presence (Fig. 4 B) and absence (Fig. 8 B) of glutamate/glycine. A number of factors might account for these differences. (a) Structurally, the NR1 M3 segment might have a greater exposure to lining the pore than the NR2C M3 segment. (b) The NR1 M3 segment may be more dynamic than the NR2C M3 segment. That is, the NR1 M3 might be constantly moving and exposing different faces of its surface, while NR2C M3 is more stable constantly exposing only one face (Banke and Traynelis, 2003). (c) The M3 segments from the two different NR1 subunits might contribute differently to pore structure with one NR1 M3 exposing one face and the other NR1 M3 exposing a different face. Together, then, the two NR1 M3s expose a wide cumulative surface. Finally, (d) the NR1 M3 segment might be less densely packed against other transmembrane segments, permitting water-accessible surfaces remote from the central access of the pore. Although our data cannot at present resolve these alternatives, alternative (d) seems unlikely since no other transmembrane segment showed accessibility deep in the pore. On the other hand, alternative (a) is consistent with the overall faster rate of MTS reactivity with substituted cysteines in NR1 M3 (Fig. 9 B), while alternatives (b) and (c) may well be explained by possible different flexibility of the M3 segments, one type of which (e.g., NR1 but not NR2) may have a higher propensity to undergo bending or kinking during gating (Sobolevsky et al., 2004).

The linker regions coupling the ligand-binding domain to the transmembrane segments, notably S1-M1 (pre-M1), M3-S2, and S2-M4 (pre-M4), line the shallow or voltage-independent portions of the outer cavity (light blue clusters in Fig. 4 A). The role of S1-M1 and M3-S2 in forming the shallow portion of the outer cavity is to a certain extent complimentary to the M3s. Indeed, their accessible surface in NR2C is wider than that in NR1, whereas in the deep part of the pore, as discussed above, the NR1 M3 has a greater accessible surface than the NR2C M3 (Fig. 4 B). An asymmetric contribution of the M1 and M3 segments from different subunits to the structure of the outer cavity argues against a strict homology to fourfold symmetric K^+ channels and supports a twofold symmetry of GluR channel (Sobolevsky et al., 2004; Tichelaar et al., 2004).

The accessible surface of M4/S2-M4 is limited and similar in both NR1 and NR2C subunits (Fig. 4). Most likely, the M4 segment is located on the back of the M1 and M3 α helices, facing the lipid of membrane. Many of the accessible positions in M4/S2-M4 that show current inhibition by MTS reagents may therefore face not the central pore but the "side entrances" to the central pore at the level of the channel-LBD linkers. The similar

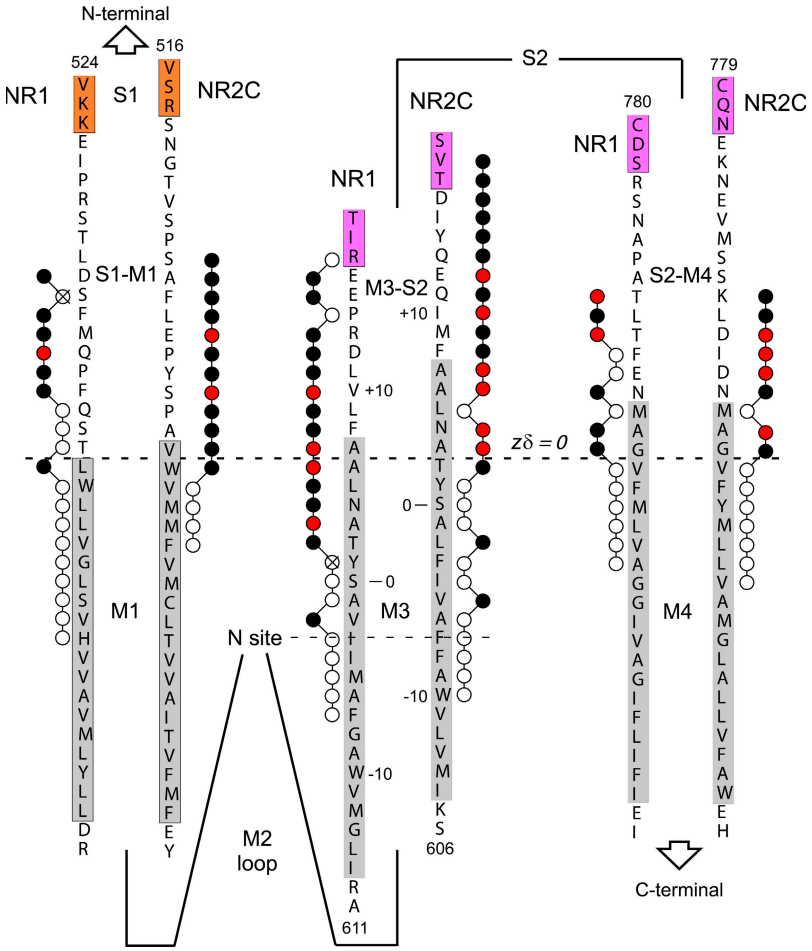

Figure 10. Vertical alignment of M1, M3, and M4 segments in NR1 and NR2C subunits. Discrete representation of reactivity of substituted cysteines with MTS reagents in the presence of agonists. MTSEA or MTSET either inhibited (black) or potentiated (red) glutamate-activated currents or did not change their amplitude (white). Some positions are also labeled red because the MTS reagent strongly altered leak current following PTrEA application. The M1, M3, and M4 segments are highlighted in gray, and the proximal parts of S1 and S2 are highlighted in orange and magenta, respectively (see Fig. 1). The dashed line separates the deep and shallow portions of the outer cavity where substituted cysteines sense and do not sense the transmembrane voltage, respectively. The most intracellular-accessible positions in M1 of NR2C as well as M4 in both NR1 and NR2C are placed at this level though we have no means to verify this positioning (since no positions show voltage-dependent reactivity).

accessibility patterns for the NR1 and NR2C M4/S2-M4 also suggests that these regions contribute similarly to channel structure. The M1 and M3 segments, on the other hand, together with the reentrant M2 loop, form the core of the channel, which shares structural similarity with K^+ channels (Wo and Oswald, 1995; Wood et al., 1995; Wollmuth and Sobolevsky, 2004). Nevertheless, the M4 segments are essential for functional NMDARs (Schorge and Colquhoun, 2003), though the basis for this remains unknown.

Vertical alignment of the transmembrane segments (Fig. 4 A and Fig. 10) illustrates the apparent staggering of the NR1 and NR2C M3 segments (Sobolevsky et al., 2002b; see Wada et al., 2006). Any vertical asymmetry of the M1 and M4 segments between the subunits, if it exists, is most likely smaller than that for the M3 segments. For example, the modification rate for L544 in NR1 is voltage dependent (Sobolevsky et al., 2002a) whereas for the homologous position V536 in NR2C it is voltage independent (Fig. 3), possibly indicating a slightly more intracellular positioning of M1 in NR1 compared with NR2C. However, additional experiments or atomic resolution structures of the channel are necessary to further address this issue.

Differential Contribution of the Transmembrane Segments in NR1 and NR2C Subunits to Gating

To address the contribution of transmembrane segments to gating, we measured steady-state accessibility and reaction rates of substituted cysteines in the presence and absence of glutamate and glycine. For an individual position, the differences observed in the presence and absence of glutamate/glycine may originate from various factors, including minor local changes in accessibility to the position. We, however, focused on patterns of changes for the entire pore-forming domains that we believe reflect global rearrangements in the channel during gating. In addition, most of the comparisons that we can make must be viewed as relative to the other regions that we are studying.

In terms of discrete accessibility derived from steady-state reactions with MTSEA, the NR2C M3 segment showed a much stronger state-dependent accessibility than the NR1 M3 segment (Fig. 2 D and Fig. 8 B). However, measurements of modification rates revealed a similar range of state-dependent differences for the NR1 and NR2C M3 segments (Fig. 9 B), consistent with both making a significant contribution to channel gating. On the other hand, the difference in discrete state

dependence reflects that modification rates for cysteines substituted in NR1 M3 are much faster than those in the NR2C M3. This result supports the idea that the NR1 and NR2C M3 segments make different contributions to the pore structure and to channel gating (Kashiwagi et al., 2002; Jin et al., 2007).

State dependence of discrete accessibility (compare Fig. 4 A and Fig. 8 A) and reaction rates (Fig. 9 B) for the S1-M1/M1 region is weaker than for the M3 segments (Thomas et al., 2006). In contrast, both steady-state accessibility and reaction rates for the S2-M4/M4 regions were nearly identical in the presence and absence of agonists, suggesting that these regions, which play an indispensable structural role in GluR channels (Wollmuth and Sobolevsky, 2004), do not significantly change their conformation during gating (see, however, Ren et al., 2003).

Lurcher Mutation-like Effects throughout the Linker Regions

The central role of M3, compared with M1 and M4, in gating is also supported by previous studies. Indeed, the most highly conserved motif in GluRs, SYTANLAAF in M3, contains a number of positions (e.g., T+2, A+3, and A+7) that show impaired or modified gating properties upon single amino acid substitution or modification of substituted cysteines by MTS reagents (Kohda et al., 2000; Taverna et al., 2000; Jones et al., 2002; Kashiwagi et al., 2002; Sobolevsky et al., 2002a, 2003; Klein and Howe, 2004). In our experimental conditions, we found that many substituted cysteines, following reaction with MTS reagents, showed potentiation of glutamate-activated currents and/or changes in leak current (Fig. 2 D, Fig. 6 A, and Table I). In analogy to the Lurcher mutation (Kohda et al., 2000), we called these Lurcher mutation-like effects and demarcated such positions as red (Figs. 4 A, Fig. 6 B, and Fig. 8 A).

The M3 segment proper is most likely α-helical. In terms of the M3 segment, red positions are clustered together (yellow clusters) and located on the opposite side to presumed pore-lining residues (deep-blue clusters in Fig. 6 B). Hence, Lurcher (A+7) and Lurcher mutation-like positions (A+3 and A+6) are located on the back side of the M3 α-helix opposite to the presumed pore-facing side. These back sides most likely contribute to interdomain interfaces that are highly dynamic during gating. Binding of MTS reagents to cysteines substituted at the contact interfaces impose restrictions on the relative movement of these domains and can sometimes shift equilibrium between the closed and open states toward the open state (potentiation of current and/or increases in leak current).

Are regions other than M3 involved in putative dynamic interdomain interfaces? Indeed, multiple red positions were also identified in the NR1 and NR2C S1-M1 (pre-M1) and S2-M4 (pre-M4) regions (yellow clusters in Fig. 4 A) that may be located at comparable vertical levels (Fig. 10). Hence, while the M3 segments from the two subunits appear to directly participate in structural rearrangements of the conduction pathway in NMDAR channel during gating, regions in S1-M1 and S2-M4 are also likely involved in this process. Indeed, mutagenesis and reactions with substituted cysteines, including Lurcher mutation-like effects, are presumably the results of disruptions at the contact interfaces between transmembrane segments M1, M3, and M4 and associated regions that are highly dynamic during gating. The nature of these interactions and their contribution to the energetics of gating however await future investigations.

We thank Drs. Stephen Traynelis, Martin Prieto, and Alexandra Corrales-Higuera for helpful discussions and/or comments on the manuscript. Michael Langis and Ronald Chiu are thanked for their assistance in handling oocytes.

This work was supported by a National Institutes of Health RO1 grant from NIMH (MH066892) (L.P. Wollmuth) and the Howard Hughes Medical Institute (grant 5003052) (M. Prodromou).

Olaf S. Andersen served as editor.

Submitted: 13 December 2006
Accepted: 30 April 2007

REFERENCES

Auerbach, A., and Y. Zhou. 2005. Gating reaction mechanisms for NMDA receptor channels. *J. Neurosci.* 25:7914–7923.

Banke, T.G., and S.F. Traynelis. 2003. Activation of NR1/NR2B NMDA receptors. *Nat. Neurosci.* 6:144–152.

Beck, C., L.P. Wollmuth, P.H. Seeburg, B. Sakmann, and T. Kuner. 1999. NMDAR channel segments forming the extracellular vestibule inferred from the accessibility of substituted cysteines. *Neuron.* 22:559–570.

Chatterton, J.E., M. Awobuluyi, L.S. Premkumar, H. Takahashi, M. Talantova, Y. Shin, J. Cui, S. Tu, K.A. Sevarino, N. Nakanishi, et al. 2002. Excitatory glycine receptors containing the NR3 family of NMDA receptor subunits. *Nature.* 415:793–798.

Clarke, R.J., and J.W. Johnson. 2006. NMDA receptor NR2 subunit dependence of the slow component of magnesium unblock. *J. Neurosci.* 26:5825–5834.

Cull-Candy, S.G., and D.N. Leszkiewicz. 2004. Role of distinct NMDA receptor subtypes at central synapses. *Sci. STKE.* 2004:re16.

Dingledine, R., K. Borges, D. Bowie, and S.F. Traynelis. 1999. The glutamate receptor ion channels. *Pharmacol. Rev.* 51:7–61.

Furukawa, H., S.K. Singh, R. Mancusso, and E. Gouaux. 2005. Subunit arrangement and function in NMDA receptors. *Nature.* 438:185–192.

Jin, L., H. Sugiyama, M. Takigawa, D. Katagiri, H. Tomitori, K. Nishimura, N. Kaur, O. Phanstiel Iv, M. Kitajima, H. Takayama, et al. 2007. Comparative studies of anthraquinone- and anthracene-tetraamines as blockers of *N*-methyl-D-aspartate receptors. *J. Pharmacol. Exp. Ther.* 320:47–55.

Jones, K.S., H.M. VanDongen, and A.M. VanDongen. 2002. The NMDA receptor M3 segment is a conserved transduction element coupling ligand binding to channel opening. *J. Neurosci.* 22:2044–2053.

Karlin, A., and M.H. Akabas. 1998. Substituted-cysteine accessibility method. *Methods Enzymol.* 293:123–145.

Kashiwagi, K., T. Masuko, C.D. Nguyen, T. Kuno, I. Tanaka, K. Igarashi, and K. Williams. 2002. Channel blockers acting at *N*-methyl-D-aspartate receptors: differential effects of mutations in the vestibule and ion channel pore. *Mol. Pharmacol.* 61:533–545.

Klein, R.M., and J.R. Howe. 2004. Effects of the lurcher mutation on GluR1 desensitization and activation kinetics. *J. Neurosci.* 24:4941–4951.

Kohda, K., Y. Wang, and M. Yuzaki. 2000. Mutation of a glutamate receptor motif reveals its role in gating and δ2 receptor channel properties. *Nat. Neurosci.* 3:315–322.

Krupp, J.J., B. Vissel, S.F. Heinemann, and G.L. Westbrook. 1996. Calcium-dependent inactivation of recombinant *N*-methyl-D-aspartate receptors is NR2 subunit specific. *Mol. Pharmacol.* 50:1680–1688.

Kuner, T., and R. Schoepfer. 1996. Multiple structural elements determine subunit specificity of Mg^{2+} block in NMDA receptor channels. *J. Neurosci.* 16:3549–3558.

Kuner, T., L.P. Wollmuth, A. Karlin, P.H. Seeburg, and B. Sakmann. 1996. Structure of the NMDA receptor channel M2 segment inferred from the accessibility of substituted cysteines. *Neuron.* 17:343–352.

Low, C.M., P. Lyuboslavsky, A. French, P. Le, K. Wyatte, W.H. Thiel, E.M. Marchan, K. Igarashi, K. Kashiwagi, K. Gernert, et al. 2003. Molecular determinants of proton-sensitive *N*-methyl-D-aspartate receptor gating. *Mol. Pharmacol.* 63:1212–1222.

Mayer, M.L. 2006. Glutamate receptors at atomic resolution. *Nature.* 440:456–462.

Monyer, H., N. Burnashev, D.J. Laurie, B. Sakmann, and P.H. Seeburg. 1994. Developmental and regional expression in the rat brain and functional properties of four NMDA receptors. *Neuron.* 12:529–540.

Ren, H., Y. Honse, B.J. Karp, R.H. Lipsky, and R.W. Peoples. 2003. A site in the fourth membrane-associated domain of the *N*-methyl-D-aspartate receptor regulates desensitization and ion channel gating. *J. Biol. Chem.* 278:276–283.

Schorge, S., and D. Colquhoun. 2003. Studies of NMDA receptor function and stoichiometry with truncated and tandem subunits. *J. Neurosci.* 23:1151–1158.

Sobolevsky, A.I., C. Beck, and L.P. Wollmuth. 2002a. Molecular rearrangements of the extracellular vestibule in NMDAR channels during gating. *Neuron.* 33:75–85.

Sobolevsky, A.I., L. Rooney, and L.P. Wollmuth. 2002b. Staggering of subunits in NMDAR channels. *Biophys. J.* 83:3304–3314.

Sobolevsky, A.I., M.V. Yelshansky, and L.P. Wollmuth. 2003. Different gating mechanisms in glutamate receptor and K^+ channels. *J. Neurosci.* 23:7559–7568.

Sobolevsky, A.I., M.V. Yelshansky, and L.P. Wollmuth. 2004. The outer pore of the glutamate receptor channel has 2-fold rotational symmetry. *Neuron.* 41:367–378.

Taverna, F., Z.G. Xiong, L. Brandes, J.C. Roder, M.W. Salter, and J.F. MacDonald. 2000. The Lurcher mutation of an α-amino-3-hydroxy-5-methyl-4-isoxazolepropionic acid receptor subunit enhances potency of glutamate and converts an antagonist to an agonist. *J. Biol. Chem.* 275:8475–8479.

Thomas, C.G., J.J. Krupp, E.E. Bagley, R. Bauzon, S.F. Heinemann, B. Vissel, and G.L. Westbrook. 2006. Probing *N*-methyl-D-aspartate receptor desensitization with the substituted-cysteine accessibility method. *Mol. Pharmacol.* 69:1296–1303.

Tichelaar, W., M. Safferling, K. Keinanen, H. Stark, and D.R. Madden. 2004. The three-dimensional structure of an ionotropic glutamate receptor reveals a dimer-of-dimers assembly. *J. Mol. Biol.* 344:435–442.

Vicini, S., J.F. Wang, J.H. Li, W.J. Zhu, Y.H. Wang, J.H. Luo, B.B. Wolfe, and D.R. Grayson. 1998. Functional and pharmacological differences between recombinant *N*-methyl-D-aspartate receptors. *J. Neurophysiol.* 79:555–566.

Wada, A., H. Takahashi, S.A. Lipton, and H.S. Chen. 2006. NR3A modulates the outer vestibule of the "NMDA" receptor channel. *J. Neurosci.* 26:13156–13166.

Watanabe, J., C. Beck, T. Kuner, L. Premkumar, and L.P. Wollmuth. 2002. DRPEER: a motif in the extracellular vestibule conferring high Ca^{2+} flux rates in NMDA receptor channels. *J. Neurosci.* 22:10209–10216.

Wo, Z.G., and R.E. Oswald. 1995. Unraveling the modular design of glutamate-gated ion channels. *Trends Neurosci.* 18:161–168.

Wollmuth, L.P., T. Kuner, P.H. Seeburg, and B. Sakmann. 1996. Differential contribution of the NR1- and NR2A-subunits to the selectivity filter of recombinant NMDA receptor channels. *J. Physiol.* 491:779–797.

Wollmuth, L.P., and A.I. Sobolevsky. 2004. Structure and gating of the glutamate receptor ion channel. *Trends Neurosci.* 27:321–328.

Wood, M.W., H.M.A. VanDongen, and A.M.J. VanDongen. 1995. Structural conservation of ion conduction pathways in K channels and glutamate receptors. *Proc. Natl. Acad. Sci. USA.* 92:4882–4886.

Wyllie, D.J., P. Behe, and D. Colquhoun. 1998. Single-channel activations and concentration jumps: comparison of recombinant NR1a/NR2A and NR1a/NR2D NMDA receptors. *J. Physiol.* 510:1–18.

Yuan, H., K. Erreger, S.M. Dravid, and S.F. Traynelis. 2005. Conserved structural and functional control of *N*-methyl-D-aspartate receptor gating by transmembrane domain M3. *J. Biol. Chem.* 280:29708–29716.